

# Journal of Mechanics of Materials and Structures

**EFFECTS OF TRANSVERSE SHEAR DEFORMATION  
ON THERMOMECHANICAL INSTABILITIES  
IN PATCHED STRUCTURES WITH EDGE DAMAGE**

Peinan Ge and William J. Bottega

**Volume 8, No. 8-10**

**October-December 2013**



## EFFECTS OF TRANSVERSE SHEAR DEFORMATION ON THERMOMECHANICAL INSTABILITIES IN PATCHED STRUCTURES WITH EDGE DAMAGE

PEINAN GE AND WILLIAM J. BOTTEGA

The problem of a patched structure under uniform thermal loading is studied, where geometric nonlinearity and shear deformation are considered. The formulation is based on the calculus of variations with propagating boundaries, and yields the governing equations, boundary conditions, matching conditions and transversality condition. Closed form analytical solutions are obtained in terms of an (unknown) membrane force parameter, the angle of rotation due to bending and the transverse displacement. Results of numerical simulations based on those solutions are presented and critical phenomena of the composite structure are unveiled. Results of the current work are compared with previously published results where transverse shear deformation was neglected. It is seen that shear deformation plays an important role in certain situations. In particular, the effects of shear deformation on the phenomena of “slingshot buckling” and “buckle trapping” are demonstrated and discussed. The influence of the relative size of the detached region and of the difference between the material properties of the base plate and of the patch (in particular, shear moduli) on the thermomechanical instabilities are elucidated.

### 1. Introduction

Patched structures are widely used in a variety of engineering systems. Such a structure consists of a secondary component adhered to a primary structure. Engineers have been using patches on aircraft in recent years to alleviate the stress intensity in the vicinity of cracks in the primary structures. It is necessary to predict and characterize the functionality of a patched structure during its servicing period. In the structures of this class, the mechanical properties of the composite structure change with respect to the properties of the patch and base components. With varying the temperature environments, with ensuing increased stress and buckling, transverse shear deformation may affect the system greatly. Therefore the characterization of the shear effect is of critical importance.

It is well known that the composite structure will eventually buckle when it is subjected to temperature change. The classic papers on thermal buckling include [Timoshenko 1925; Wittrick et al. 1953; Wahl 1944]. Karlsson and Bottega [1999] studied the presence of edge contact in patched cylindrical panels, and found that edge contact often occurs, and that it can influence the debonding behavior of the structure. Karlsson and Bottega [2000a; 2000b] and Rutgerson and Bottega [2002] subsequently studied the behavior of patched plates and layered shells, respectively, subjected to uniform temperature change. Their results showed that the structure will dynamically sling to an equilibrium configuration associated with deflections in the opposite sense of the original. The phenomenon is referred to as “slingshot buckling”

---

*Keywords:* beam, buckle trapping, buckling, patch, patched structure, contact zone, plate, slingshot buckling, stability, temperature, thermal buckling, thermal load, transverse shear deformation.

by the authors. Those studies are united and compared in [Bottega 2006b]. Recently, Bottega and Carabetta [2009] studied the detachment and separation failure of layered structures under thermal loading. The behaviors of several representative structures and loadings were studied. Carabetta and Bottega [2012; 2014] studied the instability of patched structures with edge damage where a new phenomenon referred to as “buckle trapping” was unveiled. A detailed review of the pertinent literature is presented therein. In addition, Carabetta [2011] studied the interaction of thermal buckling and detachment of patched structures. The existence of intermediate propagating contact was discussed for different bond zone sizes and edge supports. These representative results significantly advance the understanding of engineering structures. However, a more sophisticated elastic theory containing shear deformation will further elucidate the phenomena of interest.

Timoshenko [1921] was the first to introduce shear deformation as well as rotatory inertia into beam theory. Shen [1998] presented a post-buckling analysis for laminated composite plates subjected to uniform or nonuniform temperature loading. Reddy [1984] adopted higher order shear deformation in the formulation to show that the characteristics of thermal post-buckling are significantly influenced by transverse shear deformation. Aydogdu [2007] applied the Ritz method and performed an analysis of thermal buckling behavior on cross-ply laminated beams. In that work, a shear deformable theory was used in conjunction with a shape function to fulfill geometric and material constraints. Zenkour and Sobhy [2010] used a sinusoidal shear deformation plate theory to model thermal buckling phenomena of sandwich plates. Different thermal loads were applied under various configurations of the plates.

The present work focuses on the response of patched plates subjected to a uniform temperature field for a variety of support conditions and material properties. We extend the model and analysis of [Carabetta and Bottega 2014] to include transverse shear deformation. The formulations are based on [Mindlin 1951, Plate Theory], a generalization of [Timoshenko 1921, Beam Theory], and the calculus of variations. Numerical simulations are performed to elucidate representative behavior of the composite structure. Of particular interest is how the inclusion of transverse shear deformation in the overall formulation affects the response of the composite structure. In addition, the effects that the length of the patch, the proportion of Poisson’s ratio and Young’s modulus between the patch and the base plate have on the behavior of the structure are also examined.

## 2. Problem statement

In this work, we study the instability of a patched structure with a preexisting detached region emanating from each edge of the patch. We advance the work of [Carabetta and Bottega 2014] and include the effect of transverse shear deformation to examine its influence on critical phenomena. In the formulation we allow for three configurations: (1) no contact of the debonded segments of the substructures; (2) the “free” edge of the debonded segment of the patch maintains sliding contact with the base plate (“edge contact”); (3) a contact zone (a region of sliding contact) adjacent to the bonded region. Each of these configurations are shown in Figure 1.

The thin patched plate is comprised of two substructures: a base plate of half-span length  $L$ , and a patch of half-span  $L_p$  centrally and partially adhered to the base structure (Figure 2). The thicknesses of the base plate and the patch are  $h_b$  and  $h_p$ , respectively. The coordinate  $x$  originates at the centerspan and runs along the reference surface—the upper surface of the base plate. All the length scales are

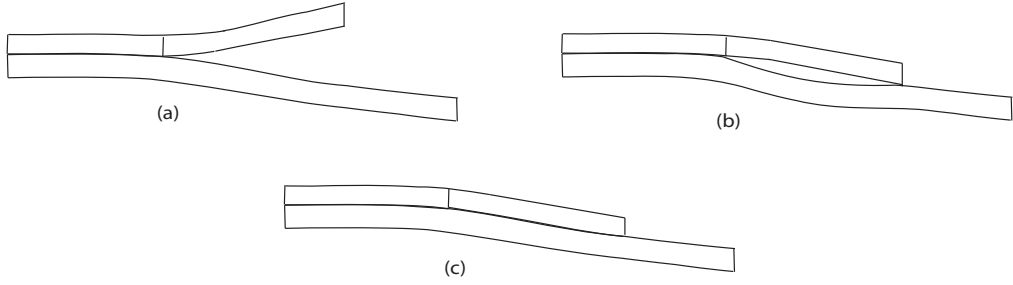


**Figure 1.** Deformed plate showing various configurations: (a) panel with no contact of debonded segments; (b) plate with edge contact of debonded segments; (c) plate with full contact of debonded segments of patch plate and base.

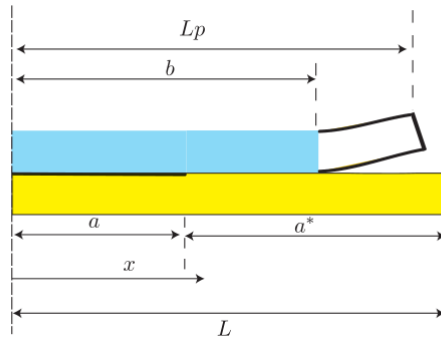


**Figure 2.** Half-span of structure.

normalized with respect to the half-length of the base plate and other pertinent parameters are normalized in accordance with [Bottega and Carabetta 2009]. Thus, for the structure of interest, the half-span length of the base plate is  $L = 1$ . The structure is mathematically partitioned into three domains: the *bond zone*  $S_1 : x \in [0, a]$ , the *contact zone*  $S_2 : x \in [a, b]$  and the *lift zone*  $S_3 : x \in [b, 1]$ . The functions  $w(x)$  and  $w_p(x)$  (positive downward) represent the normalized transverse displacements of the base plate and of the patch, respectively. The functions  $u(x)$  and  $u_p(x)$  (positive outward from centerspan) denote the corresponding normalized in-plane displacements of material particles located at the centroid of the base plate and of the patch, respectively. Correspondingly, the functions  $\phi(x)$  and  $\phi_p(x)$  represent the angle of rotation of the cross section due to bending for the base plate and of the patch, respectively. In addition, the functions  $\gamma(x)$  and  $\gamma_p(x)$  represent the shear angles of the base plate and of the patch, respectively.

Paralleling the developments in [Carabetta and Bottega 2014], the membrane strain of the base plate and of the patch,  $e_i(x)$  and  $e_p(x)$ , respectively, are given by

$$e_i = u'_{bi} + \frac{1}{2}w'_{bi}{}^2 - \alpha_b \Theta \quad (i = 1, 2, 3), \tag{1}$$

$$e_p = u'_{p2}{}^2 + \frac{1}{2}w'_{p2}{}^2 - \alpha_p \Theta, \tag{2}$$

where  $(\ )' = d(\ )/dx$  and  $\alpha_b, \alpha_p$  are described in what follows. We next adopt the normalized temperature scale of [Rutgerson and Bottega 2002; Carabetta and Bottega 2014]:

$$\Theta = \alpha \frac{\bar{\Theta} - \bar{\Theta}_0}{\bar{\Theta}_0}, \quad (3)$$

$$\alpha_b = \bar{\alpha}_b \bar{\Theta}, \quad \alpha_p = \bar{\alpha}_p \bar{\Theta} \quad (\text{plane stress}), \quad (4)$$

$$\alpha_b = \bar{\alpha}_b \bar{\Theta}(1 + \nu), \quad \alpha_p = \bar{\alpha}_p \bar{\Theta}(1 + \nu) \quad (\text{plane strain}), \quad (5)$$

where the parameters  $\bar{\Theta}$  and  $\bar{\Theta}_0$  represent the present dimensional temperature and the reference temperature of the system, respectively, and  $\nu$  is Poisson's ratio. The nondimensional coefficients of thermal expansion of the base plate and patch,  $\bar{\alpha}_b$  and  $\bar{\alpha}_p$  respectively, are defined in terms of their dimensional counterparts,  $\alpha_b$  and  $\alpha_p$ , in (4) and (5).

Paralleling the developments in [Carabetta and Bottega 2014], but now incorporating transverse shear deformation, we next formulate an energy functional in terms of the membrane energies, bending energies and shear energies of each substructure for each segment of the base panel and of the patch, and we also include constraint functionals which match the transverse displacements in the contact zone and the transverse and in-plane displacements and the angle of rotation due to bending in the bond zone. We thus formulate the energy functional  $\Pi$  as

$$\Pi = \sum_1^3 (U_B^{(i)} + U_{Bp}^{(i)} + U_M^{(i)} + U_{Mp}^{(i)} + U_S^{(i)} + U_{Sp}^{(i)}) - \Lambda \quad (6)$$

where

$$U_B^{(i)} = \int_{S_i} \frac{1}{2} D_b \kappa_i^2 dx, \quad U_{Bp}^{(i)} = \int_{S_i} \frac{1}{2} D_p \kappa_{pi}^2 dx \quad (i = 1, 2, 3) \quad (7)$$

are the bending energies in the base plate and patch in region  $S_i$ ,

$$U_M^{(i)} = \int_{S_i} \frac{1}{2} C_b e_i^2 dx, \quad U_{Mp}^{(i)} = \int_{S_i} \frac{1}{2} C_p e_{pi}^2 dx \quad (i = 1, 2, 3) \quad (8)$$

are the membrane energies in the base plate and patch in region  $S_i$ . Further

$$U_S^{(i)} = \int_{S_i} \frac{1}{2} G_b \gamma_i^2 dx, \quad U_{Sp}^{(i)} = \int_{S_i} \frac{1}{2} G_p \gamma_{pi}^2 dx \quad (i = 1, 2, 3) \quad (9)$$

are the shear energies in the base plate and in the patch in region  $S_i$ . The constraint functional  $\Lambda$  in (6) is given by

$$\Lambda = \sum_1^2 \int_{S_i} \sigma_i (w_{pi} - w_i) dx + \int_{S_1} \tau (u_{p1}^* - u_1^*) dx + \int_{S_1} \lambda (\phi_{p1}^* - \phi_1^*) dx. \quad (10)$$

In (7)–(10),  $D_b$  and  $D_p$  are the nondimensional bending stiffnesses of the base plate and the patch, respectively,  $C_b$  and  $C_p$  are the corresponding nondimensional membrane stiffnesses, and  $G_b$  and  $G_p$  are the nondimensional shear stiffnesses. In addition,  $\sigma_i$  represents the interfacial normal stress,  $\tau$  is the interfacial shear stress, and  $\lambda$  is the interfacial moment couple. According to [Mindlin 1951, Plate

Theory; Timoshenko 1921, Beam Theory; Bottega 2006a], where a shear correction and rotatory inertia are considered, the strain-displacement relation is given by

$$\frac{dw}{dx} = \phi + \gamma, \quad (11)$$

$$\gamma = \frac{V}{kGh}, \quad (12)$$

where  $w$  is the transverse displacement,  $\phi$  is the angle of rotation due to bending and  $\gamma$  is the transverse shear angle of the cross section. In (12), the parameter  $G$  is the shear modulus and  $V$  is the transverse shear force. In addition,  $k$  is the “shape factor” or “shear coefficient” of the structure, which depends on the shape of the cross section. In the past decades, the shear coefficients for various cross sections of beams were derived. Examples of related work may be found in [Mindlin 1951; Cowper 1966; Ritchie et al. 1973; Hutchinson 1981; Wittrick 1986]. Incorporating (11) into the development through Equations (6)–(10), the problem is expressed in terms of the in-plane displacement,  $u(x)$ , the transverse displacement,  $w(x)$ , and the angle of rotation due to bending,  $\phi(x)$ . The parameters shown in the above formulation of the total potential energy of the system are defined in terms of their dimensional versions as follows:

$$\begin{aligned} x &= \bar{x}/\bar{L}, & D_b &= 1, \\ u(x) &= \bar{u}(\bar{x})/\bar{L}, & C_b &= \bar{C}_b/\bar{D}_b, \\ w(x) &= \bar{w}(\bar{x})/\bar{L}, & D_p &= \bar{D}_p/\bar{D}_b, \\ \phi(x) &= \bar{\phi}(\bar{x}), & C_p &= \bar{C}_p/\bar{D}_b, \\ G_b &= k_b \bar{G}_b \bar{h}_b \bar{L}^2 / \bar{D}_b, & G_p &= k_p \bar{G}_p \bar{h}_p \bar{L}^2 / \bar{D}_b, \\ \sigma_i &= \bar{\sigma}_i \bar{L}^3 / \bar{D}_b, & \tau &= \bar{\tau} \bar{L}^3 / \bar{D}_b, \\ h_b &= \bar{h}_b / \bar{L}, & \lambda &= \bar{\lambda} \bar{L}^2 / \bar{D}_b, \\ h_p &= \bar{h}_p / \bar{L}, & L &= 1, \end{aligned} \quad (13)$$

where length scales have been normalized with respect to the dimensional half-span  $\bar{L}$  of the base plate. Invoking the principle of stationary potential energy, which is described in the present context as  $\delta\Pi = 0$ , we take the appropriate variations and allow the boundary  $b$  to vary along with the displacements. This results in the corresponding governing equations, boundary and matching conditions, and transversality condition. After eliminating the Lagrange multipliers, we arrive at the self-consistent equations and conditions for the composite structure presented next.

**2.1. Governing equations.** Adopting the procedure presented in [Carabetta and Bottega 2014], we first obtain the relation

$$N_1^* = N_2 = N_3 = -N_0 = \text{constant}, \quad N_{p2} = N_{p3} = 0, \quad (14)$$

where  $N_0$  is yet to be determined. With this important result, the problem is recast into a mixed formulation, expressed in terms of the transverse displacement,  $w(x)$ , the angle of rotation due to bending,  $\phi(x)$ , and the uniform membrane force,  $N_0$ .

The equations of transverse motion and rotation then take the form

$$\begin{aligned} D^* \phi''_{b1} + (G_b + G_p)(w'_{b1} - \phi_{b1}) &= 0, \\ -N_0 w''_{b1} + (G_b + G_p)(w'_{b1} - \phi_{b1})' &= 0, \quad x \in [0, a]. \end{aligned} \tag{15}$$

We next rearrange the above equations, eliminate  $w_{b1}$  and decouple the governing equations in terms of the angle of rotation due to bending,  $\phi_{b1}$ , and the uniform membrane force,  $N_0$ . Applying the same procedure for other regions gives the following governing equations. Hence,

$$g^* \phi'''_{b1} + N_0 \phi'_{b1} = 0 \quad (0 \leq x \leq a), \tag{16}$$

$$g_3 \phi'''_{b2} + N_0 \phi'_{b2} + D_p \phi''_{p2} = 0 \quad (a \leq x \leq b), \tag{17}$$

$$g_3 \phi'''_{b3} + N_0 \phi'_{b3} = 0 \quad (b \leq x \leq 1), \tag{18}$$

$$g_4 \phi'''_{p3} = 0 \quad (b \leq x \leq L_p), \tag{19}$$

where

$$g^* = D^* \left( 1 - \frac{N_0}{G_b + G_p} \right), \quad g_3 = D_b \left( 1 - \frac{N_0}{G_b} \right), \quad g_4 = D_p \left( 1 - \frac{N_0}{G_p} \right), \tag{20}$$

$$w''_{b1}(x) = -\frac{D^*}{G_b + G_p} \phi''_b + \phi_b, \quad w'_{b2}(x) = -\frac{D_b}{G_b} \phi''_{b2} + \phi_{b2}, \quad w'_{b3}(x) = -\frac{D_b}{G_b} \phi''_{b3} + \phi_{b3}, \tag{21}$$

$$w'_{p2}(x) = -\frac{D_p}{G_p} \phi''_{p2} + \phi_{p2}, \quad w'_{p3}(x) = -\frac{D_p}{G_p} \phi''_{p3} + \phi_{p3}. \tag{22}$$

**2.2. Boundary and matching conditions.** The associated boundary and matching conditions are obtained from the variational operation as

$$\phi_{b1}(0) = 0, \quad \phi''_{b1}(0) = 0, \quad \phi_{b3}(1) = 0, \quad w_{b3}(1) = 0, \quad \phi'_{p3}(L_p) = 0, \quad \phi''_{p3}(L_p) = 0, \tag{23}$$

$$\begin{aligned} M_\lambda(a) &= [D^* \phi'_b - D_b \phi'_{b2} - D_p \phi'_{p2}]_{x=a}, & \phi_{b1}(a) &= \phi_{b2}(a) = \phi_{p2}(a), \\ [g^* \phi''_{b1} + N_0 \phi_{b1}]_{x=a} &= [g_3 \phi''_{b2} + N_0 \phi_{b2} + D_p \phi''_{p2}]_{x=a}, & w_{b1}(a) &= w_{b2}(a) = w_{p2}(a), \end{aligned} \tag{24}$$

$$\begin{aligned} \phi'_{b2}(b) &= \phi'_{b3}(b), & \phi'_{p2}(b) &= \phi'_{p3}(b), \\ \phi_{b2}(b) &= \phi_{b3}(b), & \phi_{p2}(b) &= \phi_{p3}(b), \\ [g_3 \phi''_{b2} + N_0 \phi_{b2} + D_p \phi''_{p2}]_{x=b} &= [g_3 \phi''_{b3} + N_0 \phi_{b3} + D_p \phi''_{p3}]_{x=b}, \\ w_{b2}(b) &= w_{b3}(b) = w_{p3}(b) = w_{p2}(b) \end{aligned} \tag{25}$$

where

$$M_\lambda = m^* \Theta + \left( \rho^* + \frac{1}{2} h_b \right) N_0. \tag{26}$$

The parameter  $M_\lambda$  in the matching condition is denoted as the transverse loading parameter, which is first introduced by Karlsson and Bottega [2000a], from which the external thermal loading enters the problem for the composite structure. The two components of the loading parameter compete with each other when they have opposite sign, which is central to the “slingshot buckling” and other related issues presented in [Bottega 2006b]. The parameters  $m^*$  and  $\rho^*$  are given in Appendix A. Finally, integrating

the strain-displacement relations and imposing the boundary and matching conditions for the in-plane displacements result in the integrability condition

$$u_{b2}(1) - u_b(0) = -N_0 \left( \frac{1-a}{C_b} + \frac{a^*}{C_p} \right) + \left( 1 - a + a \frac{n^*}{C^*} \right) \Theta - \left( \frac{1}{2} h_b + \rho^* \right) \phi_b(a) - \frac{1}{2} \int_0^a w_b'^2 dx - \frac{1}{2} \int_a^b w_{b2}'^2 dx - \frac{1}{2} \int_b^1 w_{b3}'^2 dx. \quad (27)$$

**2.3. Transversality condition.** The partially debonded structure discussed on page 503 (see especially Figure 2) is divided into 3 segments — bonded zone, contact zone and lift zone. The location of the boundary between the contact zone and the lift zone is determined by the corresponding transversality condition that is derived by taking the appropriate variations and allowing the boundary  $b$  to vary along with the displacements. This condition reduces to the equality of the total angular displacement of the patch and the base plate at the contact zone boundary. Therefore, a propagating contact boundary may occur only if the following condition is satisfied

$$w'_{b3}(b) = w'_{p3}(b), \quad (28)$$

$$w'_{b3}(b) > 0, \quad (29)$$

where (29) is added to prohibit penetration of the patch to the base plate. If (28) and (29) are not satisfied, the system will possess either a full contact zone ( $b = L_p$ ), no contact zone ( $b = a$ ), or edge point contact, whichever possesses the lowest system energy.

**2.4. Condition for (full) contact or lift.** To establish whether full contact between, or lift off of, the detached segment of the patch and the base plate occurs for clamped-fixed, we establish a kinematic criterion based on physical arguments. For lift off to occur, a pseudo inflection point must occur at the bond zone boundary,  $x = a$ . This can be characterized by the product of the gradients of total rotations of the composite plate in the bond zone and in the contact zone, evaluated at the bond zone boundary. That is,

$$J_a \equiv w''_1(a) \cdot w''_2(a). \quad (30)$$

If

$$J_a < 0, \quad (31)$$

a full contact zone is possible. If

$$J_a > 0, \quad (32)$$

lift is possible. The above is coupled with the sense of the deflections when making an assessment.

**2.5. Stability criterion.** For a given value of the applied thermal loading, if multiple equilibrium configurations exist, it is necessary to determine which of the configurations are stable and which are unstable. In this regard, we utilize the second variation of the potential energy functional to assess the stability of each equilibrium configuration (the approach implemented in [Karlsson and Bottega 2000a]). The configuration is considered stable if the second variation of the total potential is positive definite ( $\delta^2 \Pi > 0$ ). We adopt the approach discussed in [Karlsson and Bottega 2000b], in which the transverse displacements



and the axial strains are perturbed via their coefficients. Doing this, we obtain the second variation of the total potential energy in the following form,

$$\delta^2 \Pi = \hat{F}(\delta M_\lambda)^2 + \zeta(\delta N_0)^2 \quad (33)$$

where  $\Pi$  is the total potential energy,  $\delta$  is the variational operator,

$$\zeta = \frac{1}{2} \left( \frac{a}{C^*} + \frac{a^*}{C_b} \right) \quad \text{and} \quad \hat{F} = \hat{F}(N_0, a, b). \quad (34)$$

As discussed in [Carabetta and Bottega 2014], the form of the function  $\hat{F}$  depends on the particular support conditions for the specific structure. Since  $\zeta > 0$ , the requirement of positive definiteness of the second variation reduces to the stability criterion

$$\hat{F} > 0. \quad (35)$$

In this regard, a configuration is stable when (35) is satisfied. The function  $\hat{F}$  is therefore referred to as the stability function.

### 3. Analysis

Solving Equations (16)–(19), subject to the boundary and matching conditions of Equations (23)–(25), yields the solutions for the angle of rotation due to bending in each region. The solutions are presented for two extreme support conditions: hinged-fixed and clamped-fixed ends. The general solutions to the governing equations of Section 2, Equations (16)–(19), are found to be

$$\phi_{b1}(x) = C_1 + C_2 \cos(K_b x) + C_3 \sin(K_b x), \quad (36)$$

$$\phi_{b2}(x) = A_1 \cosh(\mu_1 x) + A_2 \sinh(\mu_1 x) + A_3 \sin(\beta_1 x) + A_4 \cos(\beta_1 x) + A_5, \quad (37)$$

$$\phi_{p2}(x) = P_1[A_1 \cosh(\mu_1 x) + A_2 \sinh(\mu_1 x)] + P_2[A_3 \sin(\beta_1 x) + A_4 \cos(\beta_1 x)] + A_5, \quad (38)$$

$$\phi_{b3}(x) = C_4 + C_5 \cos(K_{b3} x) + C_6 \sin(K_{b3} x). \quad (39)$$

The parameters  $\mu_1$ ,  $K_b$ ,  $K_{b3}$ ,  $\beta_1$ ,  $P_1$ , and  $P_2$  are given in Appendix B. Note that, for both support conditions, the rotations for the base plate and patch within the contact zone are not identical ( $P_1 \neq 1$ , and  $P_2 \neq 1$ ) when the shear deformation is included. The relations between transverse deflection and the angle of rotation due to bending are described by (21) and (22). The expressions for the constants  $C_1, \dots, C_6$  and  $A_1, \dots, A_5$  depending on the specific support conditions imposed at  $x = 1$ , are cumbersome, and are omitted for brevity. It is noted that the equations presented above reduce to the solutions for a perfectly intact structure in the limiting scenario when  $G_b, G_p \rightarrow \infty$ .

With the analytical solution and stability criterion established, we next present the results of numerical simulations based on these solutions.

### 4. Results and discussion

The purpose of this study is to demonstrate the influence of transverse shear deformation on the behavior of the structure under thermal loading. This is done by comparing results of the present model with those found in [Carabetta and Bottega 2014] using the corresponding model neglecting transverse shear

deformation. In this section, numerical results are presented for structures with hinged-fixed edges and for structures with clamped-fixed ends, under uniform thermal loading. The effect of changing the shear modulus of the patch and base plate will be analyzed to reveal characteristic behavior. The corresponding thickness ratio is taken as  $h_0 = 1$  and the ratio of coefficient of thermal expansion of the patch to the base is  $\alpha_p^0 = 0.5$ , which are consistent with those used in [Carabetta and Bottega 2014].

**4.1. Hinged ends.** We first consider the structure with hinged-fixed supports. That is, the edges of the base plate are hinged with respect to rotation and fixed with respect to in-plane translation. For such support conditions, no contact zone exists when the partially detached structure deflects upward, due to the lack of an inflection point or pseudo-inflection point. When in this configuration, the partially detached structure is equivalent to the intact structure having the same bond zone size in terms of global stiffness and energy. This is consistent with previous studies [Bottega and Carabetta 2009; Carabetta and Bottega 2012; Carabetta 2011]. In contrast, the structure possesses a full contact zone when it deflects downwards. Thus, as discussed in [Carabetta and Bottega 2014], a “dual nature” exists for a partially debonded structure with hinged-fixed supports. In order to appropriately capture the overall behavior of the structure under thermal loading, results of simulations for a structure with no contact zone ( $b = a$ ) and a structure having a full contact zone ( $b = L_p$ ) are presented together. To show the effect of transverse shear on the behavior of the structure, two cases are presented: (1) equal shear stiffness for the two layers; (2) unequal shear stiffness for the base plate and patch.

Case 1: *Equal shear stiffness* ( $G_b = G_p$ ). The shear stiffnesses of the base plate and of the patch are identical, for equal thickness, if both the Young’s modulus and Poisson’s ratio are equal, per the well-known relation

$$G = \frac{E}{1 + \nu}. \quad (40)$$

The results for a structure possessing a bond zone of length  $a = 0.6$  and a patch length  $L_p = 0.9$  are displayed in Figures 3 and 5. The papers [Carabetta and Bottega 2012; 2014; Carabetta 2011] studied the behavior of the same structure with the transverse shear deformation neglected. The results displayed in Figure 3 are regenerated according to [Carabetta and Bottega 2014]. The load-deflection path is shown in Figure 3(b) as the applied temperature change as a function of the center point deflection. The membrane force, total energy and stability function are shown as a function of the applied temperature change in parts (a), (c) and (d) of Figure 3, with the shear deformation neglected. The corresponding results, with shear deformation accounted for, are displayed in Figure 4. Comparison of Figures 3 and 4 shows virtually no difference in the response of the structure, indicating that the transverse shear has little effect for the case when  $G_b = G_p$ . In these figures, red color indicates the stable equilibrium configurations and blue color indicates the unstable equilibrium configurations. It is seen from Figure 4(b) that, as the temperature change is increased from zero, the structure initially deflects upward and continues to do so until the critical temperature is achieved,  $\Theta_{cr} = 2.2$ . At this point, the configuration associated with Branch 1 becomes unstable and the structure slingshots to an alternate stable configuration on Branch 2. As the structure deflects downward, the detached “flap” of the patch comes into contact with the base plate when  $w(0) \geq 0$  and a full contact configuration appears. Thus the rightmost path shown in Figure 4(b) is dismissed on physical grounds.

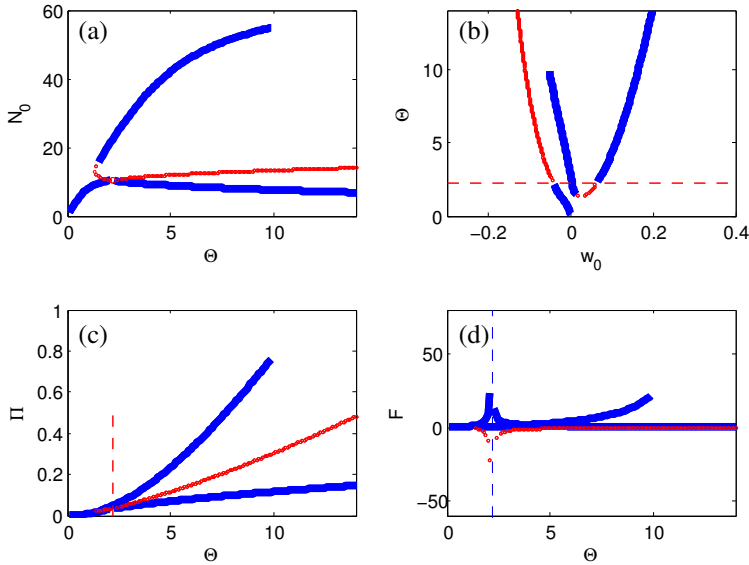


**Figure 3.** Behavior of hinged-fixed structure with shear deformation neglected, for a fully lifted flap, with  $a = 0.6$ ,  $L_p = 0.9$ : (a) membrane force vs. temperature difference; (b) temperature difference vs. center-span transverse deflection; (c) total potential energy vs. temperature difference; (d) stability function vs. temperature difference. Red circles represent stable configurations and blue lines indicate unstable ones.

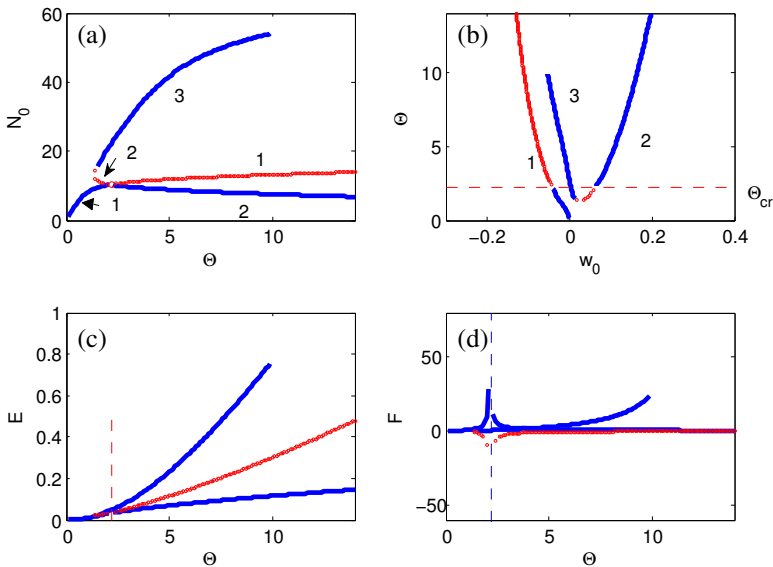


**Figure 4.** Behavior of hinged-fixed structure,  $G_b = G_p$ , for a fully lifted flap, with  $a = 0.6$ ,  $L_p = 0.9$ : (a) membrane force vs. temperature difference; (b) temperature difference vs. center-span transverse deflection; (c) total potential energy vs. temperature difference; (d) stability function vs. temperature difference. Red circles represent stable configurations and blue lines indicate unstable ones.

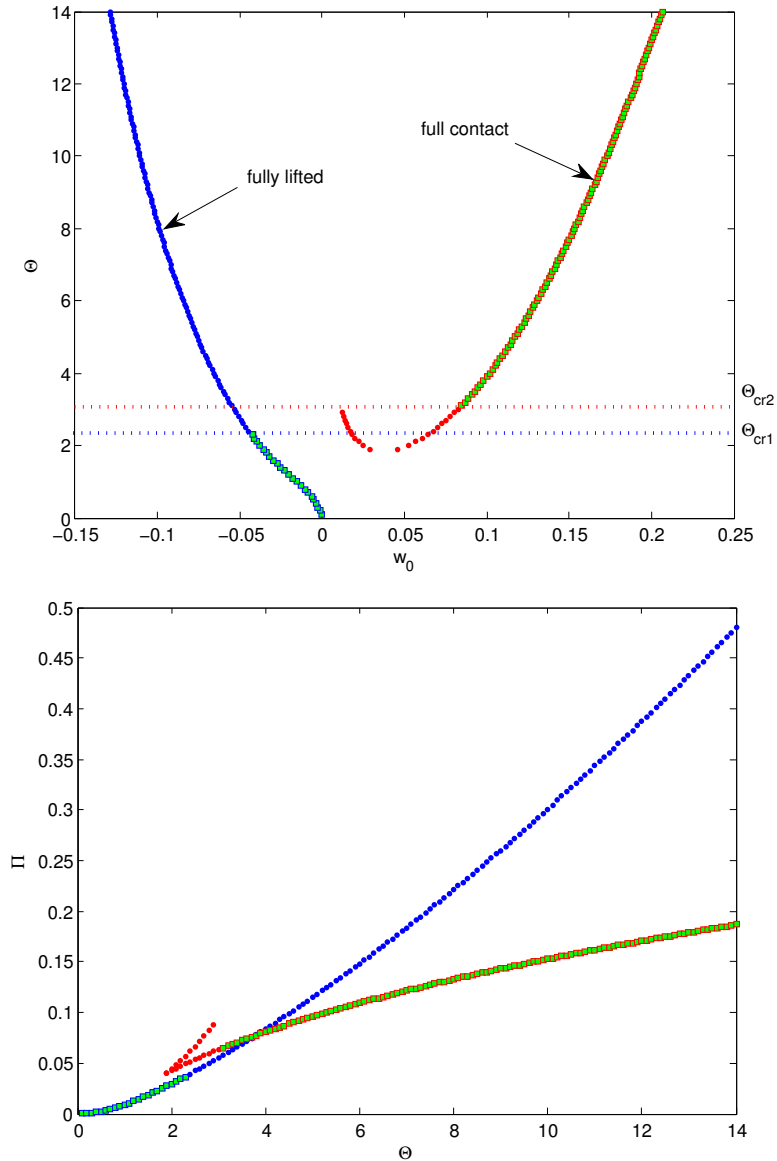


**Figure 5.** Thermal load-deflection paths (top) and total energy as a function of the temperature change (bottom) for hinged-fixed total structure with  $G_b = G_p$ ,  $a = 0.6$ , and  $L_p = 0.9$ .

Figure 5 displays profiles of the temperature difference vs. centerspan displacement and the total energy vs. temperature difference, respectively for the structure. In these figures, red color corresponds to the full contact configuration and blue color to the fully lifted configuration. The squares indicate the stable equilibrium positions and the dots indicate the unstable positions. In these figures, the gap between the critical temperatures of the two configurations is shown. When the structure switches from the fully lifted configuration to the full contact configuration, there is no stable equilibrium position in

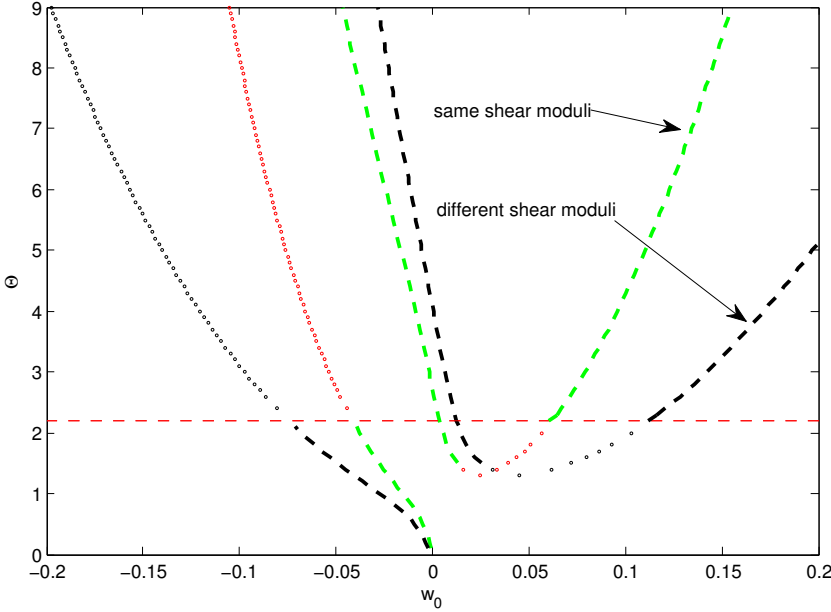


**Figure 6.** Comparison of thermal load-deflection paths for hinged-fixed structures with  $G_p \neq G_b$  ( $\nu_b/\nu_p = 0.3/0.2$ ) with those for  $G_p = G_b$ ,  $a = 0.6$ ,  $L_p = 0.9$ . Dashed lines represent stable configurations and circles indicate the unstable configurations.

either configuration. Thus, the structure is trapped between the two. This phenomenon, called *buckle trapping*, was established by Carabetta and Bottega [2012; 2014], who proposed the existence of an energy cusp, and hence a stable equilibrium configuration, when  $w = 0$  ( $\Theta_{cr1} \leq \Theta \leq \Theta_{cr2}$ ). Simulations for a bond zone of half-length  $a = 0.8$  with the same patch length are also studied, but the results are omitted for brevity. However, It is observed that the “buckle trapping” phenomenon exists even with the shear correction for this case. It is thus seen that, in this regard, the effects of transverse shear deformation are not apparent when the base plate and the patch possess equal shear stiffness.

*Case 2: Unequal shear stiffnesses ( $G_b \neq G_p$ ).* We next consider the case when the base plate and the patch possess unequal shear stiffness ( $G_b \neq G_p$ ). Selected results of simulations based on the solutions discussed in Section 3 are presented in what follows.

Results for a structure possessing a bond zone of half-length  $a = 0.6$  and a patch half-length  $L_p = 0.9$  are displayed in Figures 6 and 7. A comparison of the thermal load-deflection paths is displayed in Figure 6 for both cases: (1) equal shear stiffness ( $G_b/G_p = 1$ ) and (2) unequal shear stiffness ( $G_b/G_p = 2.2/2.6$ ), between the base plate and the patch. The profile for equal shear stiffness was already discussed under Case 1. In Figure 6, the black curves correspond to  $G_b \neq G_p$  case and the colored curves correspond to  $G_b = G_p$  case. The dashed lines indicate stable equilibrium configurations and the circles indicate the unstable states. Although the critical temperature for both cases is the same ( $\Theta_{cr} = 2.2$ ), the deflection corresponding to the structure with unequal shear stiffnesses is seen to be much larger than that of the structure with equal shear stiffnesses, as  $\Theta$  increases. Thus, the effect of shear deformation on the behavior of the structure is apparent in this case.

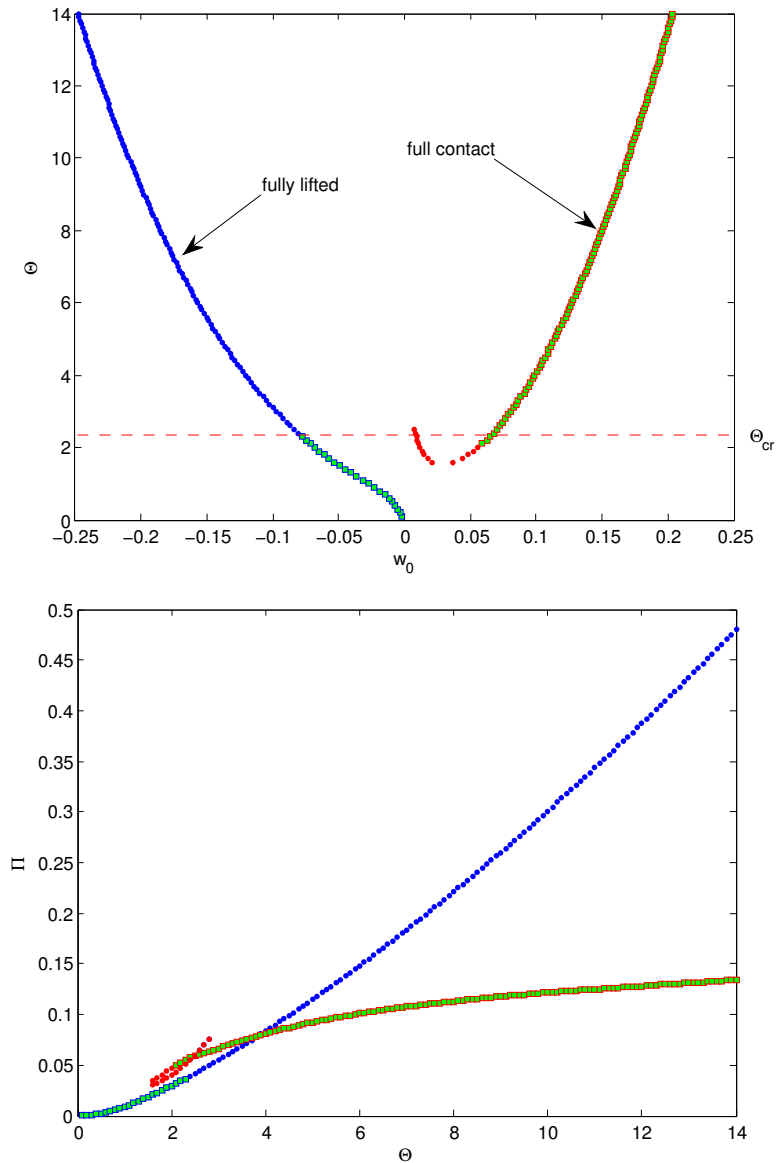


**Figure 7.** Thermal load-deflection paths (top) and total energy as a function of the temperature change (bottom) for hinged-fixed structure with  $\nu_b/\nu_p = 0.3/0.2$ ,  $a = 0.6$ ,  $L_p = 0.9$ .

Figure 7 shows the dual load-deflection curve and the total energy profile as a function of the temperature change (both the full contact and fully lifted configurations are presented). It was shown previously, for Case 1, that at the critical temperature, the structure buckles from the fully lifted configuration, and buckle trapping occurs before it reaches the full contact configuration. However, it is seen from Figure 7 that the partially detached structure buckles from a fully lifted configuration to a full contact configuration at the critical temperature  $\Theta_{cr} = 2.2$  where it is stable for the full contact configuration.

Thus, the buckle trapping phenomenon disappears for this case. We also examined the partially debonded structure with differing shear stiffnesses for a bond zone size  $a = 0.8$  and observed similar behavior. The results are omitted for brevity. Comparing these results to those for the case of a structure with equal shear stiffnesses, we observe that the “buckle trapping” phenomenon does not occur when the base plate and the patch possess unequal shear stiffnesses for the case considered. This is in contrast to what was predicted by Carabetta and Bottega [2014], with the transverse shear neglected. We next proceed to the case of structures with clamped-fixed edges under uniform temperature change.

**4.2. Clamped ends.** We next consider the situation when the edges of the base-plate are clamped-fixed. That is, when the edges of the structure are clamped with respect to rotation and fixed with respect to both transverse and in-plane translation. The general behavior of the whole structure will be seen to be notably different from that of the structure with hinged-fixed supports described earlier. It was established in [Bottega and Carabetta 2009; Carabetta and Bottega 2014; Carabetta 2011] that a propagating intermediate contact zone is possible for certain bond zone sizes. For the present case, we demonstrate the existence of fully lifted, full contact, intermediate contact and edge contact configurations, with transverse shear effect included. As the structure deflects upward, edge contact may occur as discussed by Karlsson and Bottega [1999] for patched cylindrical panels. It is observed for the present case that, in contrast to what was observed for hinged supports, contact occurs in prebuckling and lift occurs in postbuckling. When intermediate contact occurs, the transversality condition (28) and its caveat (29) are used to determine the location of the contact zone/lift zone boundary under a certain temperature change. In this section, some representative examples will be presented to demonstrate the variety of behaviors. The first example is for the case when the shear stiffnesses of the base plate and the patch are equal.

Case 1: *Equal shear stiffness* ( $G_b = G_p$ ). Results for a structure possessing a bond zone of half-length  $a = 0.6$  and a patch half-length  $L_p = 0.9$  are presented in Figures 8–11. For a structure with clamped ends, edge contact as well as full contact configurations are possible when the structure deflects upward. Unlike the situation when shear deformation is neglected, it is found presently that, when shear deformation is accounted for, an edge contact configuration may occur when the structure deflects upward. In situations when the patched structure has more than one admissible configuration for a given bond zone size, the one with the lowest total potential energy will be considered as the “preferred” configuration for a particular patch and base structure [Carabetta and Bottega 2012; 2014]. The total energies for three different configurations (full contact, no contact and edge contact) are presented in Figure 8. Based on the results of the junction rotation gradient product,  $J_a$ , presented in Figure 9, it is observed that at  $\Theta = 2.4$ , the full contact configuration is no longer valid as the sign of  $J_a$  becomes the same. The structure, thus, has two possible configurations — no contact or edge contact. However, it is seen from Figure 8 that the edge contact configuration has a lower potential energy at this temperature. Thus, we take the edge contact configuration as the “preferred” configuration for the system. As the temperature increases, the total energy of the edge contact configuration exceeds that of the no contact configuration, and the patched structure switches to the no contact configuration at  $\Theta = 5.5$ , with the patch lifting away from the base plate.

The final load-deflection profile and the total energy of the structure (only stable configurations) are presented in Figures 10 and 11, respectively. It is noticed that the structure first possesses a full contact zone and then, at  $\Theta = 2.4$  it “jumps” to edge contact, and then to no contact configuration when  $\Theta \geq 5.5$ . The simulation results for a bond zone half-length of  $a = 0.8$  are summarized in Table 1. At this point, it

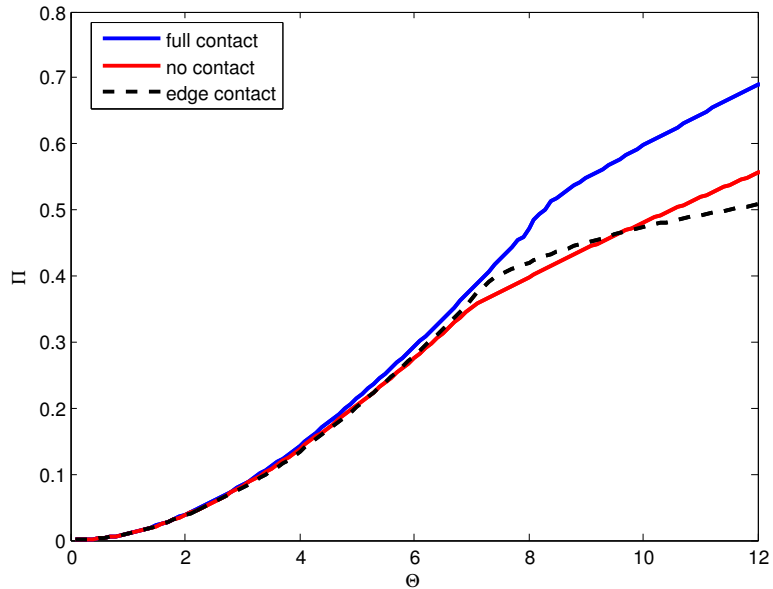


**Figure 8.** Comparison of total energy (full contact, fully lifted and edge contact) vs. temperature difference for clamped-fixed structure with  $G_b = G_p$ ,  $a = 0.6$ ,  $L_p = 0.9$ .

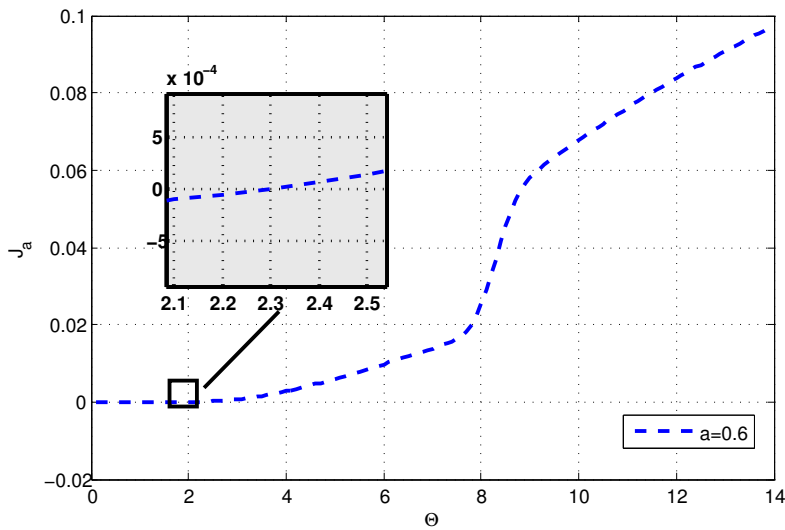


**Figure 9.** Junction parameter,  $J_a$ , as a function of the temperature difference for clamped-fixed structure with  $G_b = G_p$ ,  $a = 0.6$ ,  $L_p = 0.9$ .

is concluded that, for the case with equal shear stiffness, the patched plate possesses three configurations during the temperature increases: full contact, edge contact and no contact. Intermediate contact does not occur.

Next, let us consider the case when the base plate and the patch have different shear stiffnesses.



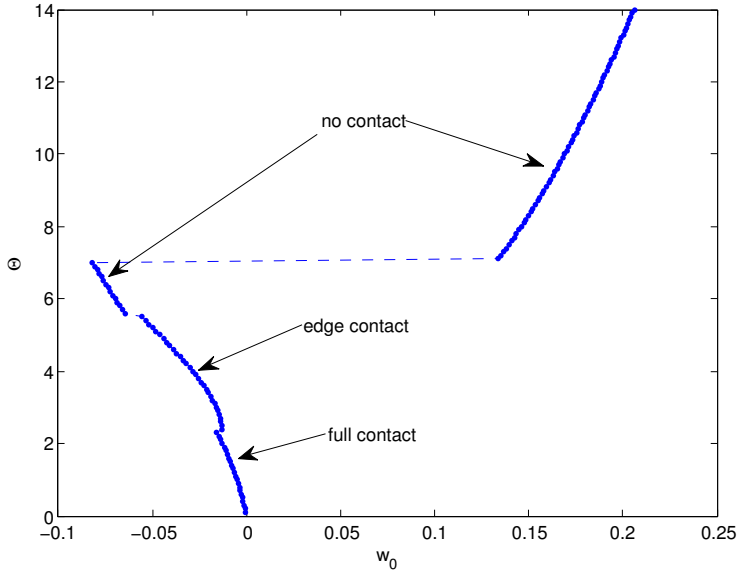


**Figure 10.** Thermal load-deflection paths for clamped-fixed structure with  $G_b = G_p$ ,  $a = 0.6$ ,  $L_p = 0.9$ .

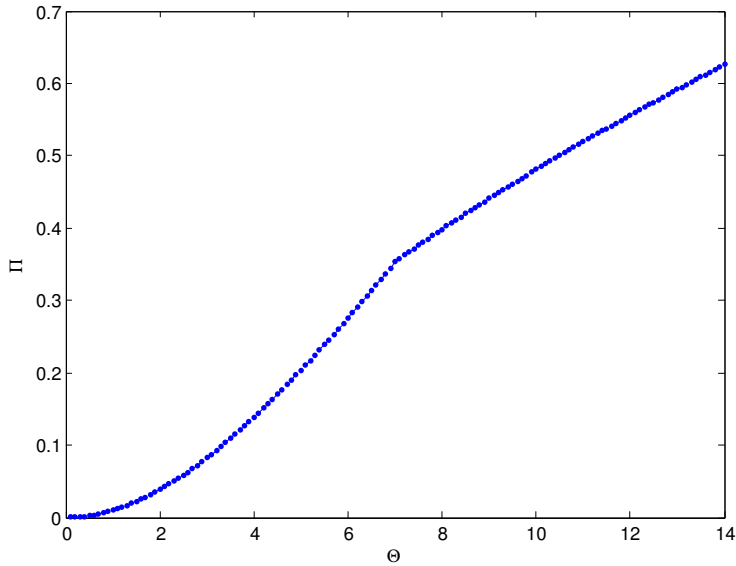


**Figure 11.** Clamped-fixed structure,  $G_b = G_p$ , total energy vs. temperature difference;  $a = 0.6$ ,  $L_p = 0.9$ .

Case 2: *Unequal shear stiffnesses* ( $G_b \neq G_p$ ). In this section, we consider the case when the shear stiffnesses of the patch and of the base plate are unequal. We remark that this is equivalent to the substructures possessing different Poisson's ratios and/or different Young's moduli per the well known relation (40).

	$E_b = E_p$			$\nu_b = \nu_p$		$\frac{E_b = E_p}{\nu_b = \nu_p}$
	$\frac{\nu_b = 0.3}{\nu_p = 0.25}$	$\frac{\nu_b = 0.25}{\nu_p = 0.3}$	$\frac{\nu_b = 0.1}{\nu_p = 0.3}$	$\frac{E_b}{E_p} = 0.1$	$\frac{E_b}{E_p} = 10$	$G_b = G_p$
$a = 0.8$	Full $\Downarrow \theta = 4.3$ No	Full $\Downarrow \theta = 4.2$ No	Full $\Downarrow \theta = 4.2$ No	Full $\Downarrow \theta = 3.3$ No	Full $\Downarrow \theta = 2.5$ No	Full $\Downarrow \theta = 4$ No
$a = 0.6$	Full $\Downarrow \theta = 1.8$ Edge $\Downarrow \theta = 5.6$ No	Full $\Downarrow \theta = 2$ Edge $\Downarrow \theta = 5.5$ No	Full $\Downarrow \theta = 2.6$ Edge $\Downarrow \theta = 5.5$ No	Full $\Downarrow \theta = 3.2$ No	Full $\Downarrow \theta = 2.5$ No	Full $\Downarrow \theta = 2.4$ Edge $\Downarrow \theta = 5.5$ No

**Table 1.** Summary of the simulation results for clamped-fixed edge. “Full” represents “full contact”, and likewise for “Edge” and “No”.

As discussed in the previous section, the analytical solution for this situation differs substantially from that of the case with equal shear stiffness. It is anticipated some interesting behaviors of the patched structure will be unveiled.

1. *Different Poisson’s ratios and equal Young’s moduli.* Results for a structure possessing a bond zone size of  $a = 0.6$  and a patch half-length  $L_p = 0.9$  are presented in Figures 12–15. To identify the existence of the contact zone and edge contact configurations, we combine the results of the junction rotation gradient product,  $J_a$ , in Figure 13 with those for the total potential energy of the three configurations presented in Figure 12. In Figure 13, the full contact configuration is no longer valid when the sign of  $J_a \equiv J_a \equiv w_1''(a) \cdot w_2''(a)$  changes. Thus, the structure “jumps” to a configuration with edge contact when the temperature achieves the value  $\Theta = 1.7$ . At this point, the system assumes a configuration with edge contact, which has a lower total potential energy. The structure then switches to a configuration with no contact, when  $\Theta = 5.3$ . The trend is similar to that for the case of equal shear stiffness, however the critical “jump” temperature changes substantially. The results displayed in Figures 14 and 15 show the “actual” load-deflection paths and the total energy, respectively. It is noticed that the structure initially possesses a full contact zone, but at  $\Theta = 1.7$ , it “jumps” to a configuration with edge contact, and then to a configuration with no contact when  $\Theta = 5.3$ . Results are also obtained for the case of a contact zone length of  $a = 0.8$  and for different Poisson’s ratios of the two layers. Characteristic behavior for this case is summarized in Table 1 along with those for a structure with a bond zone half-length of  $a = 0.6$ . Based on these results, we see that for different Poisson’s ratios, the structure follows a similar trend as for  $a = 0.8$ . We next consider the effect of Young’s modulus on the behavior of the structure.

2. *Different Young’s moduli and equal Poisson’s ratio.* Different Young’s moduli will result in different shear stiffnesses between the patch and the base plate, per (40). However, unlike for Poisson’s ratio, Young’s modulus will also affect the membrane energy and bending energy of the system.

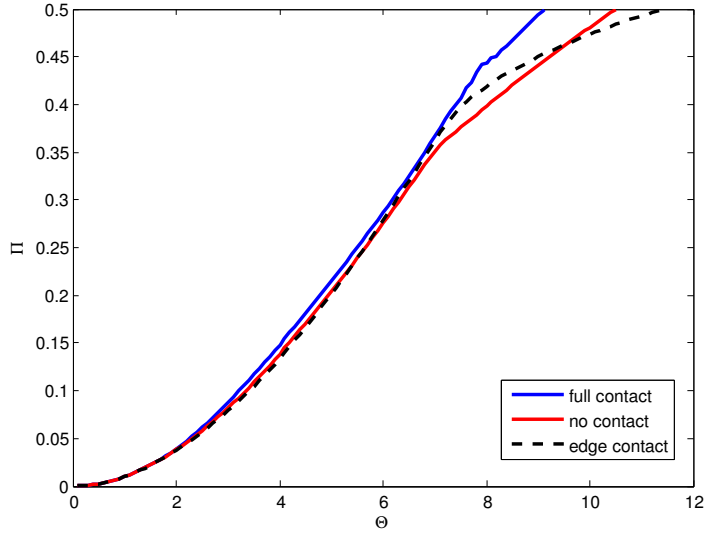


**Figure 12.** Comparison of total energy (full contact, fully lifted and edge contact) as a function of the temperature difference for clamped-fixed structure with  $\nu_b/\nu_p = 0.3/0.2$ ,  $a = 0.6$ ,  $L_p = 0.9$ .

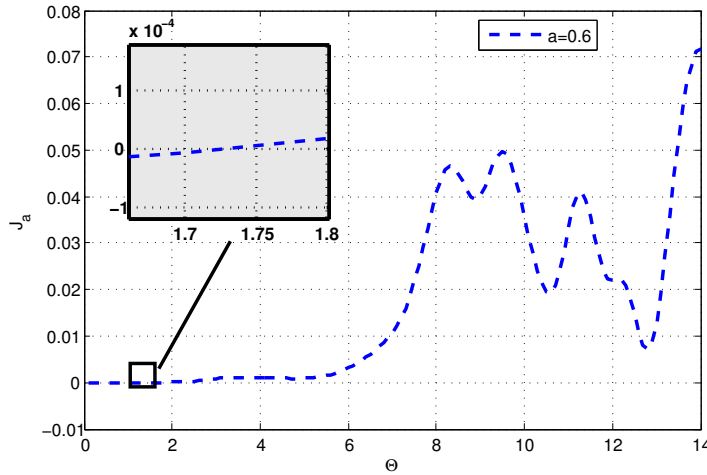


**Figure 13.** Junction parameter,  $J_a$ , as a function of the temperature difference for clamped-fixed structure with  $\nu_b/\nu_p = 0.3/0.2$ ,  $a = 0.6$ ,  $L_p = 0.9$ .

It is therefore essential to study the behavior of the patched structure when Young’s modulus for the patch and that of the base plate differ. Results for the case when the ratio of Young’s modulus of the base plate to that of the patch is  $E_b/E_p = 0.1$  are displayed in Figures 16–18 for a structure that possesses a bond zone half-length of  $a = 0.6$ . The transversality condition is then examined to check the existence of an intermediate contact zone and to determine the location of the contact point. It is seen from Figure 16 that when the structure deflects upward, it will initially possess a full contact zone until the critical temperature is reached. At this temperature, the structure buckles downward. We note

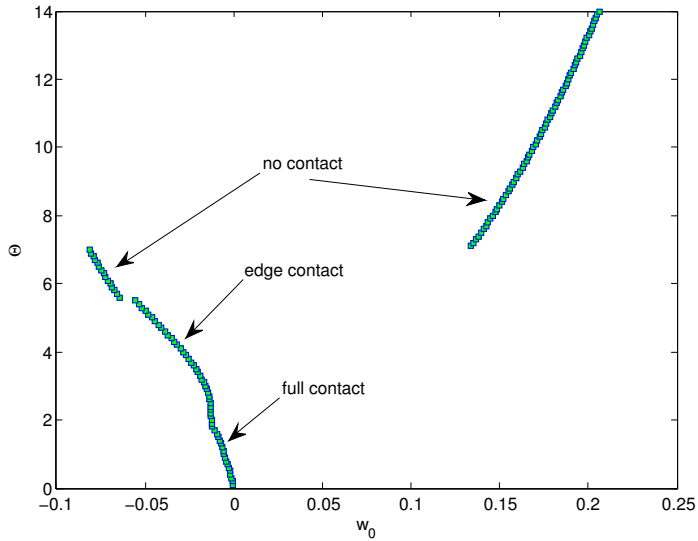


**Figure 14.** Thermal load-deflection paths for clamped-fixed structure with  $\nu_b/\nu_p = 0.3/0.2$ ,  $a = 0.6$ ,  $L_p = 0.9$ .

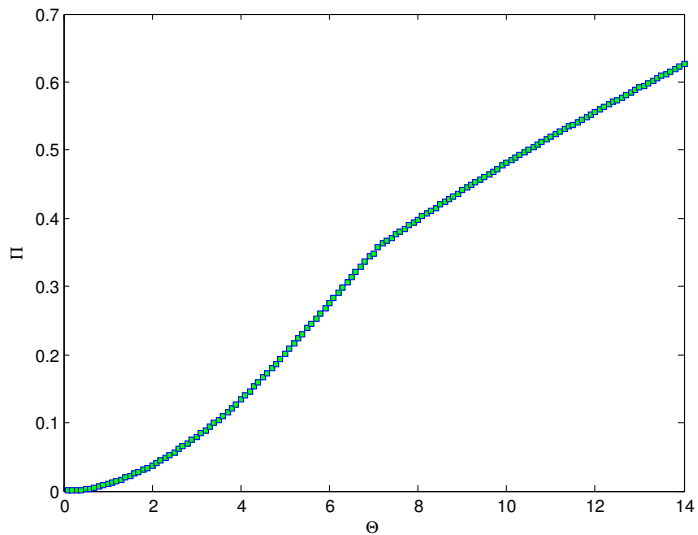


**Figure 15.** Clamped-fixed structure,  $\nu_b/\nu_p = 0.3/0.2$ , total energy vs. temperature difference;  $a = 0.6$ ,  $L_p = 0.9$ .

that, for this range of temperatures, the sign of  $J_a$  is negative, which indicates that the structure will not possess a contact zone when it deflects downward. For this case, we also find that there is no edge contact configuration during the temperature increase. Therefore, at the critical temperature, the structure slingshots from a configuration with full contact to a configuration with no contact. The “actual” load-deflection curve and the total energy profile (stable configurations) of the system are shown in Figures 17

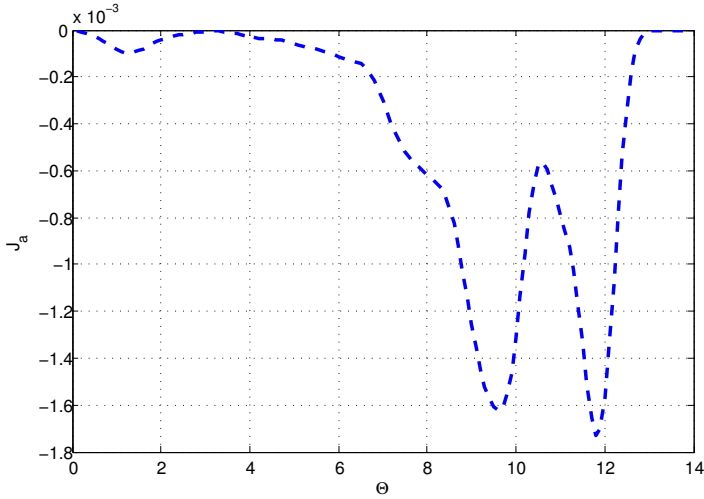


**Figure 16.** Junction parameter,  $J_a$ , as a function of the temperature difference for clamped-fixed structure with  $E_b/E_p = 0.1$ ,  $a = 0.6$ ,  $L_p = 0.9$ .

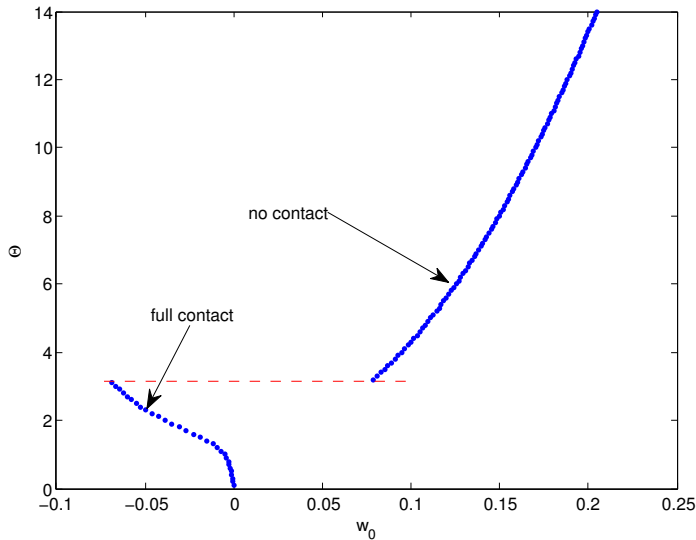


**Figure 17.** Clamped-fixed structure,  $E_b/E_p = 0.1$ , center-span displacement vs. temperature difference;  $a = 0.6$ ,  $L_p = 0.9$ .

and 18, respectively. It is seen that, as the temperature is increased, the structure first possesses a full contact zone and then “jumps” to a no contact configuration at  $\Theta = 3.2$ .

A summary of characteristic behavior, and its relation to bond zone size, Young’s modulus, and Poisson’s ratio of the layers is presented in Table 1. The morphological “transition” temperatures, at which the structure will switch from one type of configuration to another type of configuration (e.g., full contact, edge contact, no contact) are shown separately for each case. It is seen that edge contact will not occur, for the larger bond zone size considered,  $a = 0.8$ . In contrast, it is seen that edge contact often occurs for

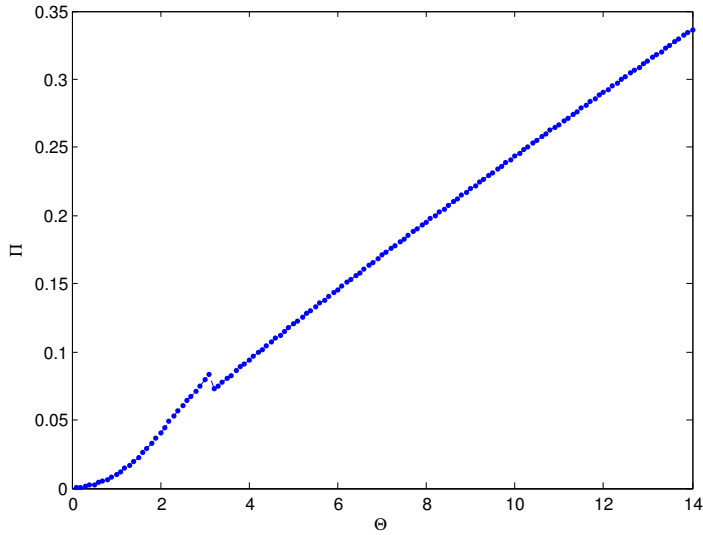


**Figure 18.** Clamped-fixed structure,  $E_b/E_p = 0.1$ , total energy vs. temperature difference;  $a = 0.6$ ,  $L_p = 0.9$ .

the other bond zone size considered,  $a = 0.6$ , except for the case when the two layers have the same Young's modulus, but different Poisson's ratio. Thus, the morphology of the partially detached patched structure is very sensitive to the material properties of the constituent structures.

## 5. Conclusions

The current work includes transverse shear deformation and, in this regard, advances on specific prior studies concerning thermal instabilities in patched beam-plates with partial edge detachment. The resulting governing equations, internal and external boundary conditions, transversality condition and stability criterion are derived using a variational formulation. Closed form analytical solutions to the governing equations are determined and simulations based on these solutions are performed. The associated analysis and numerical simulations reveal representative and critical behavior of the partially detached structure under uniform temperature change for both hinged-fixed and clamped-fixed edges. The influence of transverse shear on critical behavior is assessed through examination of these results. For structures with hinged-fixed supports, when the shear moduli of the patch and of the base plate are equal, it is observed that transverse shear deformation has minimal influence for the representative cases considered. It is also seen that the phenomenon of "buckle-trapping" still exists (first revealed in a prior study using a classical model—no transverse shear deformation). However, behavior is altered and "buckle trapping" is not observed to occur when the shear moduli of the substructures are unequal. This is in contrast to prior results predicted using the simpler (no transverse shear) model. One concludes from this that the simpler model for the structure, that which neglects transverse shear deformation, is inadequate in this case. Structures with clamped-fixed supports allow for several possible local configurations of the detached segment of patch and base plate: full contact, no contact and edge contact. Those that are not physically realizable are disqualified, based on local kinematic conditions and the relative magnitudes of

the total potential energies for each case. For these structures, we also consider the situation where the patch and base plate possess the same shear stiffnesses but have different Poisson's ratios and different Young's moduli. Results for structures with clamped-fixed supports are seen to differ significantly from those of previous studies using the simpler (no transverse shear) model. For the cases considered here, propagating intermediate contact zone configurations (predicted by the model without shear deformation) are not observed. However, edge contact configurations not observed with the simpler model, are often seen to occur for structures with relatively small bond zone sizes in the results of the present analysis. To conclude, based on the results of the present study, it is found that transverse shear deformation generally has substantial influence on critical behavior of the structures of interest.

### Appendix A. Stiffnesses of composite structure in bond zone

$$A^* = D_b + D_p + (h_b/2)^2 C_b + (h_p/2)^2 C_p, \quad (\text{A.1})$$

$$B^* = (h_p/2) C_p - (h_b/2) C_b, \quad (\text{A.2})$$

$$C^* = C_p + C_b, \quad D^* = A^* - \rho^* B^*, \quad (\text{A.3})$$

$$\rho^* = B^*/C^*, \quad (\text{A.4})$$

$$n^* = C_b \alpha_b + C_p \alpha_p, \quad (\text{A.5})$$

$$\mu^* = \frac{1}{2} h_p C_p \alpha_p - \frac{1}{2} h_b C_b \alpha_b, \quad (\text{A.6})$$

$$m^* = \mu^* - \rho^* n^*. \quad (\text{A.7})$$

The quantity  $\rho^*$  is seen to give the transverse location of the centroid of the composite structure with respect to the reference surface.

### Appendix B. Solution parameters

$$\mu_1 = \frac{\hat{b} - \sqrt{R}}{-2\hat{a}}, \quad \beta_1 = \frac{\hat{b} + \sqrt{R}}{-2\hat{a}}, \quad P_1 = \frac{1 - \frac{D_b}{G_b} \alpha_1^2}{1 - \frac{D_p}{G_p} \alpha_1^2}, \quad P_2 = \frac{1 - \frac{D_b}{G_b} \beta_1^2}{1 - \frac{D_p}{G_p} \beta_1^2} \quad (\text{general case}), \quad (\text{B.1})$$

$$\mu_1 = \sqrt{\frac{G_b}{D_b}}, \quad \beta_1 = \sqrt{\frac{N_0}{D_b(2 - \frac{N_0}{G_b})}}, \quad P_1 = -1, \quad P_2 = 1 \quad (\text{special case } G_p = G_b), \quad (\text{B.2})$$

$$\hat{b} = -(D_b + D_p - N_0(\frac{D_b}{G_b} + \frac{D_p}{G_p})), \quad \hat{c} = -N_0, \quad K_b = \sqrt{N_0/g^*}, \quad (\text{B.3})$$

$$\hat{a} = \frac{D_b D_p}{G_b G_p} (G_b + G_p - N_0), \quad R = \hat{b}^2 - 4\hat{a}\hat{c}, \quad K_{b3} = \sqrt{N_0/g_3}. \quad (\text{B.4})$$

### References

- [Aydogdu 2007] M. Aydogdu, "Thermal buckling analysis of cross-ply laminated composite beams with general boundary conditions", *Compos. Sci. Technol.* **67**:6 (2007), 1096–1104.
- [Bottega 2006a] W. J. Bottega, *Engineering vibrations*, CRC Press, Boca Raton, FL, 2006.
- [Bottega 2006b] W. J. Bottega, "Sling-shot buckling of composite structures under thermo-mechanical loading", *Int. J. Mech. Sci.* **48**:5 (2006), 568–578.

- [Bottega and Carabetta 2009] W. J. Bottega and P. M. Carabetta, “On the detachment of patched panels under thermomechanical loading”, *J. Mech. Mater. Struct.* **4**:7–8 (2009), 1227–1250.
- [Carabetta 2011] P. M. Carabetta, *On the interaction of thermal buckling and debonding of patched structures*, Ph.D. thesis, Rutgers University, New Brunswick, 2011, available at <http://rucore.libraries.rutgers.edu/rutgers-lib/33593/>.
- [Carabetta and Bottega 2012] P. M. Carabetta and W. J. Bottega, “On the interaction of thermally induced buckling and debond propagation in patched structures”, *J. Appl. Mech.* **79**:6 (2012), 061012.
- [Carabetta and Bottega 2014] P. M. Carabetta and W. J. Bottega, “Thermo-mechanical instabilities in patched structures with edge damage”, *Int. J. Non-linear Mech.* **58** (2014), 89–98.
- [Cowper 1966] G. R. Cowper, “The shear coefficient in Timoshenko’s beam theory”, *J. Appl. Mech.* **33**:2 (1966), 335–340.
- [Hutchinson 1981] J. R. Hutchinson, “Transverse vibrations of beams, exact versus approximate solutions”, *ASME J. Appl. Mech.* **48**:4 (1981), 923–928.
- [Karlsson and Bottega 1999] A. M. Karlsson and W. J. Bottega, “The presence of edge contact and its influence on the debonding of patched panels”, *Int. J. Fract.* **96**:4 (1999), 383–406.
- [Karlsson and Bottega 2000a] A. M. Karlsson and W. J. Bottega, “On thermal buckling of patched beam-plates”, *Int. J. Solids Struct.* **37**:34 (2000), 4655–4690.
- [Karlsson and Bottega 2000b] A. M. Karlsson and W. J. Bottega, “Thermo-mechanical response of patched plates”, *AIAA Journal* **38**:6 (2000), 1055–1062.
- [Mindlin 1951] R. D. Mindlin, “Influence of rotary inertia and shear on flexural motions of isotropic elastic plates”, *ASME J. Appl. Mech.* **18** (1951), 31–38.
- [Reddy 1984] J. N. Reddy, “A simple higher-order theory for laminated composite plates”, *J. Appl. Mech.* **51**:4 (1984), 745–752.
- [Ritchie et al. 1973] R. O. Ritchie, J. F. Knott, and J. R. Rice, “On the relationship between critical tensile stress and fracture toughness in mild steel”, *J. Mech. Phys. Solids* **21**:6 (1973), 395–410.
- [Rutgerson and Bottega 2002] S. E. Rutgerson and W. J. Bottega, “Thermo-elastic buckling of layered shell segments”, *Int. J. Solids Struct.* **39**:19 (2002), 4867–4887.
- [Shen 1998] H.-S. Shen, “Thermomechanical post-buckling analysis of imperfect laminated plates using a higher-order shear-deformation theory”, *Comput. Struct.* **66**:4 (1998), 395–409.
- [Timoshenko 1921] S. P. Timoshenko, “LXVI. On the correction for shear of the differential equation for transverse vibrations of prismatic bars”, *The London, Edinburgh, and Dublin Philosophical Magazine and Journal of Science* **41**:245 (1921), 744–746.
- [Timoshenko 1925] S. P. Timoshenko, “Analysis of bi-metal thermostats”, *J. Opt. Soc. Am.* **11**:3 (1925), 233–255.
- [Wahl 1944] A. M. Wahl, “Analysis of Valverde thermostat”, *J. Appl. Mech.* **11** (1944), A183–A189.
- [Wittrick 1986] W. H. Wittrick, “Analytical, three-dimensional elasticity solutions to some plate problems, and some observations on Mindlin’s plate theory”, *Int. J. Solids Struct.* **23**:4 (1986), 441–464.
- [Wittrick et al. 1953] W. H. Wittrick, D. M. Myers, and W. R. Blunden, “Stability of a bimetallic disk”, *Quart. J. Mech. Appl. Math.* **6**:1 (1953), 15–31.
- [Zenkour and Sobhy 2010] A. M. Zenkour and M. Sobhy, “Thermal buckling of various types of FGM sandwich plates”, *Composite Structures* **93**:1 (2010), 93–102.

Received 16 Jul 2013. Revised 26 Sep 2013. Accepted 27 Oct 2013.

PEINAN GE: [pelange@eden.rutgers.edu](mailto:pelange@eden.rutgers.edu)

Department of Mechanical and Aerospace Engineering, Rutgers University, 98 Brett Road, Piscataway, NJ 08854-8058, United States

WILLIAM J. BOTTEGA: [bottega@rci.rutgers.edu](mailto:bottega@rci.rutgers.edu)

Department of Mechanical and Aerospace Engineering, Rutgers University, Campus at New Brunswick, 98 Brett Road, Piscataway, NJ 08854-8058, United States



# JOURNAL OF MECHANICS OF MATERIALS AND STRUCTURES

[msp.org/jomms](http://msp.org/jomms)

Founded by Charles R. Steele and Marie-Louise Steele

## EDITORIAL BOARD

ADAIR R. AGUIAR University of São Paulo at São Carlos, Brazil  
KATIA BERTOLDI Harvard University, USA  
DAVIDE BIGONI University of Trento, Italy  
IWONA JASLUK University of Illinois at Urbana-Champaign, USA  
THOMAS J. PENCE Michigan State University, USA  
YASUhide SHINDO Tohoku University, Japan  
DAVID STEIGMANN University of California at Berkeley

## ADVISORY BOARD

J. P. CARTER University of Sydney, Australia  
R. M. CHRISTENSEN Stanford University, USA  
G. M. L. GLADWELL University of Waterloo, Canada  
D. H. HODGES Georgia Institute of Technology, USA  
J. HUTCHINSON Harvard University, USA  
C. HWU National Cheng Kung University, Taiwan  
B. L. KARIHALOO University of Wales, UK  
Y. Y. KIM Seoul National University, Republic of Korea  
Z. MROZ Academy of Science, Poland  
D. PAMPLONA Universidade Católica do Rio de Janeiro, Brazil  
M. B. RUBIN Technion, Haifa, Israel  
A. N. SHUPIKOV Ukrainian Academy of Sciences, Ukraine  
T. TARNAI University Budapest, Hungary  
F. Y. M. WAN University of California, Irvine, USA  
P. WRIGGERS Universität Hannover, Germany  
W. YANG Tsinghua University, China  
F. ZIEGLER Technische Universität Wien, Austria

**PRODUCTION** [production@msp.org](mailto:production@msp.org)

SILVIO LEVY Scientific Editor

---

See [msp.org/jomms](http://msp.org/jomms) for submission guidelines.


---

JoMMS (ISSN 1559-3959) at Mathematical Sciences Publishers, 798 Evans Hall #6840, c/o University of California, Berkeley, CA 94720-3840, is published in 10 issues a year. The subscription price for 2013 is US \$555/year for the electronic version, and \$705/year (+\$60, if shipping outside the US) for print and electronic. Subscriptions, requests for back issues, and changes of address should be sent to MSP.

---

JoMMS peer-review and production is managed by EditFLOW<sup>®</sup> from Mathematical Sciences Publishers.

PUBLISHED BY

 **mathematical sciences publishers**  
nonprofit scientific publishing

<http://msp.org/>

© 2013 Mathematical Sciences Publishers

- Analysis of pull-in instability of electrostatically actuated carbon nanotubes using the homotopy perturbation method** MIR MASOUD SEYYED FAKHRABADI, ABBAS RASTGOO and MOHAMMAD TAGHI AHMADIAN 385
- Thermoelastic damping in an auxetic rectangular plate with thermal relaxation: forced vibrations** BOGDAN T. MARUSZEWSKI, ANDRZEJ DRZEWIECKI, ROMAN STAROSTA and LILIANA RESTUCCIA 403
- Worst-case load in plastic limit analysis of frame structures** YOSHIHIRO KANNO 415
- A two-dimensional problem in magnetoelastostaticity with laser pulse under different boundary conditions** SUNITA DESWAL, SANDEEP SINGH SHEORAN and KAPIL KUMAR KALKAL 441
- Rapid sliding contact in three dimensions by dissimilar elastic bodies: Effects of sliding speed and transverse isotropy** LOUIS MILTON BROCK 461
- Weight function approach to a crack propagating along a bimaterial interface under arbitrary loading in an anisotropic solid** LEWIS PRYCE, LORENZO MORINI and GENNADY MISHURIS 479
- Effects of transverse shear deformation on thermomechanical instabilities in patched structures with edge damage** PEINAN GE and WILLIAM J. BOTTEGA 501